CrossMark

Numerical investigation of off-centre binary collision of droplets in a horizontal channel

Z. Goodarzi[1] · Afshin Ahmadi Nadooshan[1] · M. Bayareh[1]

Abstract

The collision between two off-centre water droplets in horizontal channels is investigated. Three-dimensional simulations are performed for fully developed, laminar, unsteady and incompressible flow. Volume of Fluid (VOF) computational method is used to calculate the fluid flow. The first droplet is separated from the channel wall and the second one moves by the flow in the center of the channel. The effects of Weber number, Reynolds number, density ratio, viscosity ratio, the ratio of droplet size and impact factor on the elongation and maximum velocity of droplets are investigated after coalescence. A correlation coefficient is obtained for elongation according to the dimensionless parameters. The results show that the elongation curve is sinusoidal due to the tendency of droplets to achieve a spherical shape. The velocity of droplets before collision relative to the velocity of droplets after coalescence is twice.

Keywords Volume of fluid method · Droplet coalescence · Off-centre droplet · Elongation

1 Introduction

Coalescence of droplets is important in many industries, for example, coating and sintering processes, sprays, printing, food processing, combustion or the formation of rain droplets in clouds. Coalescence of droplets is started when two droplets come into contact and form a bridge and then starts to grow due to surface tension. This growth is due to viscous dissipation or inertial forces and finally the two droplets have merged to a single droplet.

Ashgriz and Givi [1] carried out an experimental study in which the coalescence efficiencies of two colliding n-Hexane fuel droplets are determined. They concluded that the Weber number is an important parameter in characterizing the outcome of the collision in that different types of collisions would occur depending on the magnitude of the local Weber number.

Hyun et al. [2] investigated two-dimensional numerical simulations of the impact and spreading of a droplet to understand particle effects on spreading dynamics of a particle-laden droplet. They did this work for to evaluate the application of inkjet printing process. Additionally, emulsification is important in many processes for production and functionalization of dispersed liquid systems. Bayareh and Mortazavi [3, 4] studied the equilibrium position of a drop in shear and pressure-driven flows using front-tracking method. They found that the final position of the drop is independent of its initial position. Krause and Fritsching [5] exhibited a correction of the standard VOF-model for multiphase flow using a separate phase indicator for every single droplet (multiple entity models).

Some researchers have conducted experimental investigations of the binary droplet collision dynamics. Qian and Law [6] investigated the droplet collision dynamics based on a series of time-resolved images of the collision event with different collision inertia and impact parameter. They studied the effect of liquid and gas properties by conducting experiments with both water and hydrocarbon droplets in environments of different gases (air, nitrogen, helium and ethylene). Wierzba [7] studied the interaction between two liquid droplets and determined values of the critical Weber number experimentally. The author concluded that an increase in Weber number in this region results in an increased percentage of droplets with regular bag type breakup for a given initial droplet diameter.

✉ Afshin Ahmadi Nadooshan
   ahmadi@eng.sku.ac.ir

[1] Faculty of Engineering, Shahrekord University, Shahrekord, Iran

Ashgriz and Poo [8] investigated the binary collision dynamics of droplets. They experimentally and theoretically showed that the critical condition for the beginning of reflexive separation occurs when the kinetic energy of these internal flows is larger than 75% of the surface energy of a nominal droplet having the same volume as the combined droplets. Seevaratnam et al. [9] investigated the deformation of oil droplets of varying viscosity adhering to a solid, rigid wall in a rectangular channel experimentally which induced by a pressure-driven, laminar flow of water. They studied the effects of initial droplet volume, flow rate and viscosity ratio on the various modes of droplet motion and deformation.

Different numerical methods have been used to study the deformation and breakup of a single liquid droplet in shear flows. Renardy [10] used VOF method to simulate the production of a droplet and illustrated that inertia can enhance elongation to break the droplet by examining Reynolds numbers in the range of 1–10. He concluded that the volumes of the daughter droplets can be larger than that in the unbounded case. Kekesi et al. [11] used VOF method to investigate the deformation and breakup of a single liquid droplet in shear flows that superimposed on uniform flow. Ioannou et al. [12] applied a Lattice Boltzmann method to study confinement effect on the dynamical behavior of a droplet immersed in an immiscible liquid subjected to a simple shear flow. They investigated the effects of capillary number and viscosity ratio to the carrier liquid, and confinement ratio. The authors concluded that increasing confinement ratio will upgrade deformation, and the maximum deformation occurs at the viscosity ratio of unity. Kathleen Feigl et al. [13] studied the effect of various geometrical, flow and fluid parameters on the characteristics of droplet production, in particular, droplet size using numerical simulations in shear flow fields.

The interaction between two bubble (and drops) suspended in a shear or pressure-driven flows have been the subject of several studies [14–19]. For example, Nobari and Tryggvason [16] studied the off-center collision of two droplets in three-dimensional simulations using front-tracking finite-difference method. They showed that the droplets coalesce permanently for small impact parameters, but a grazing collision, where the droplets coalesce and then stretch apart again, is observed for larger impact parameters. Melean and Sigalotti [17] illustrated two-dimensional numerical calculations of the head-on and off-centre binary collision dynamics of equal-sized droplets using the method of smoothed particle hydrodynamics (SPH). They investigated the effects of impact velocity and the impact parameter on the outcome of permanent coalescence. Nikolopoulos et al. [18] performed a numerical investigation of the collision of two non-central equal size droplets in a gaseous phase. They did the time evolution of

the geometrical characteristics of the ligament for different Weber numbers. They revealed that gas bubbles are trapped within the liquid phase due to the collision. Saroka et al. [19] investigated the droplet collisions without the effect of a surrounding environment in three-dimensional numerical simulations using Volume of Fluid method. They plotted regions of permanent coalescence and separation in the Weber-Reynolds number plane. Krishnan and Loth [20] investigated the boundaries that separate outcomes of the collision of two spherical droplets in a gas using different droplet viscosities and surface tensions as well as gas pressure and density.

To the best of our knowledge, binary collision of drops in a simple shear or pressure-driven flows has been performed at zero or finite Reynolds numbers. Although, some investigations considered the interaction between drops at high Reynolds numbers, but their simulations have been performed at relatively high Weber numbers (ambient fluid is in gaseous phase) [19, 20]. The primary aim of the present work is to investigate off-center interaction of two drops at moderate Reynolds numbers, $Re \sim O$ (100) for low values of Weber number. Since the number of at least 30 points across the drop diameter is needed to capture the density boundary layer, the simulation at Reynolds numbers of O (100) requires so high computational time. The second aim is to explore the combined effect of ambient fluid and initial drop velocities on the physical mechanism of the interaction at different non-dimensional governing parameters.

Understanding the mechanism of pairwise interaction of drops has a fundamental role to predict the probability of formation of clusters in suspensions or generation of churn flow in tubes, for example, motion of water liquid drops in crude oil pipelines. In the present study, the collision of two off-centre droplets in a horizontal channel is simulated in which the flow is fully developed, laminar and unsteady. The paper is organized as follows: Sect. 2 represents the numerical method governing equations. In Sect. 3, effect of different non-dimensional parameter on the interaction between two drops is presented. Concluding remarks is considered in Sect. 4.

2 Numerical method and governing equations

The flow induced by the off-centre binary collision of two equal-sized droplets is considered as three-dimensional, incompressible and laminar; the two-phase flow (phase 2 is the liquid phase, and phase 1 is the surrounding one) is mathematically expressed by the Navier–Stokes equations and the continuity equation. For identifying each phase separately a volume fraction, denoted by $\propto$, is introduced

following VOF Method. The volume fraction $\propto$ is defined as Eq. (1).

$$\propto = \frac{\text{Volume of liquid phase}}{\text{Total volume of the control volume}}. \tag{1}$$

The values of density ρ and viscosity μ are calculated using linear interpolation between the values of the two phases weighted with the volume fraction $\propto$:

$$\rho = \alpha \rho_d + (1-\alpha)\rho_g, \tag{2}$$

$$\mu = \alpha \mu_d + (1-\alpha)\mu_g, \tag{3}$$

where the $\propto$-function is equal to:

$$\propto = \begin{cases} 1, & \text{for a point inside liquid phase} \\ 0, & \text{for a point inside surrounding phase} \\ 0 < \propto < 1, & \text{for a point inside the transitional} \\ & \text{area between the two phases} \end{cases} \tag{4}$$

The transport equation for the volume fraction is defined as Eq. (5).

$$\frac{D\alpha}{Dt} = \frac{\partial \alpha}{\partial t} + u.\nabla\alpha = 0. \tag{5}$$

The details of applied numerical method have been presented in [21]. The momentum equations expressing both phases are written in the form as Eq. (6).

$$\frac{\partial(\rho\vec{u})}{\partial t} + \nabla.\left(\rho\vec{u}\otimes\vec{u} - \vec{T}\right) = \rho\vec{g} + f_\sigma \tag{6}$$

In these equations, $\vec{u}$ is the velocity, ρ and μ are the discontinuous density and viscosity fields, $\vec{T}$ is the stress tensor and f_σ is the volumetric force due to surface tension. The volumetric force f_σ is equal to:

$$f = \sigma.k.(\nabla\alpha), \tag{7}$$

The Weber and the Reynolds numbers are governing non-dimensional parameters. In off-centre collision, the droplets approach each other along parallel lines that are some distance apart. If this distance is greater than the droplet diameter D, the droplets never touch and no collision takes place. If the distance is zero, the head-on collision happens. To describe the off-center collision, a new non-dimensional parameter, called the impact parameter (I), is required. These dimensionless parameters are defined as Eq. (8).

$$We = \frac{\rho_d D U^2}{\sigma}, \quad Re = \frac{\rho_d U D}{\mu_d}, \quad I = \frac{X}{D}. \tag{8}$$

Where U is the relative velocity of the droplets at impact and X is the perpendicular distance between the lines that the droplets move along before the collision.

2.1 Numerical details of the simulated cases

In this study the numerical simulations of two water droplets collision which they are assumed as off-center is presented, while the density, the viscosity and surface tension coefficient are kept constant. The external fluid can be changed with the different condition of this issue.

Droplets have a preliminary velocity while the relative velocity is constant in all cases. The droplet which it is near the channel surface makes an angle of 45° with the x-axis, but the another droplets is situated in the middle of the channel with the initial velocity in the flow direction. The geometry and boundary conditions are presented in Fig. 1. Droplets have been located at the center of the channel in the Y-direction. Additionally, the initial velocity profiles of the droplets on X–Z plane is illustrated in Fig. 2.
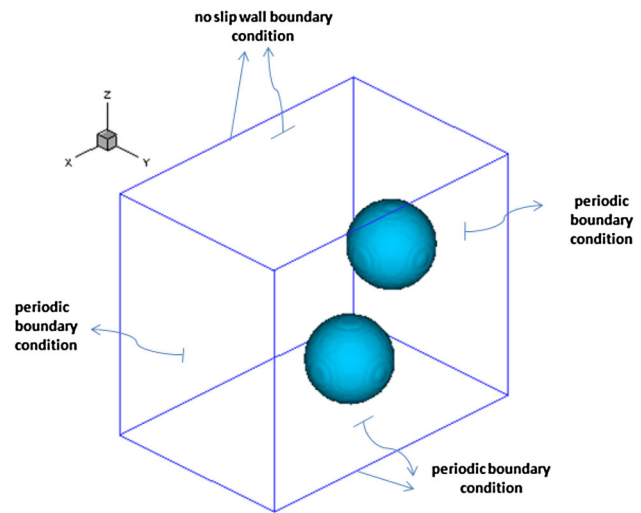

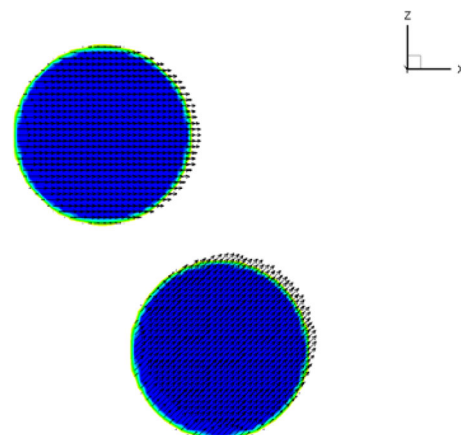**Fig. 1** The computational domain and boundary conditions

Fig. 2 The initial velocity droplet profiles on page X–Z

Table 1 Test cases examined in the present work

Case	I	$\frac{D_1}{D_2}$	$\frac{\mu_d}{\mu_g}$	$\frac{\rho_d}{\rho_g}$	We	Re
1	0.16	1	1	1	0.53	107.48
2	0.16	1	1	3	0.53	107.48
3	0.16	1	1	6	0.53	107.48
4	0.16	1	1	1	0.53	53.741
5	0.16	1	1	1	0.53	26.870
6	0.16	1	1	1	1.063	53.741
7	0.16	1	1	1	2.126	53.741
8	0.16	1	20	1	0.53	107.48
9	0.16	1	50	1	0.53	107.48
10	0.16	1.33	1	3	0.53	107.48
11	0.16	0.75	1	3	0.53	107.48
12	0.16	1	1	3	1.063	53.741
13	0.16	1	1	3	1.063	53.741

The information about droplets and review streams is shown in Table 1. The "d" and "g" indexes are related to the droplets and ambient fluid, respectively. D_1 and D_2 are referring to the droplet's diameter of channel center and the droplet in the near surface of channel, respectively. In all cases, the channel length is 3/8D, Channel width is 2/5D and Channel height is 3/2D.

3 Results and discussion

3.1 Validation

The results of the present work are compared with the results of Saroka et al. [19] performed three-dimensional numerical simulations of droplet collisions without the effect of a surrounding environment. Initial droplet diameter and relative velocity were 300 μm and 3.76 m/s, respectively. Also, $Re = 1127$ and $We = 58$.

The cell size of the droplet diameter is considered with 40 cells per diameter. Figures 3 and 4 show the comparison between the results of Saroka et al. [19] and current results. It can be seen that the qualitative and quantitative results match well with the work done.
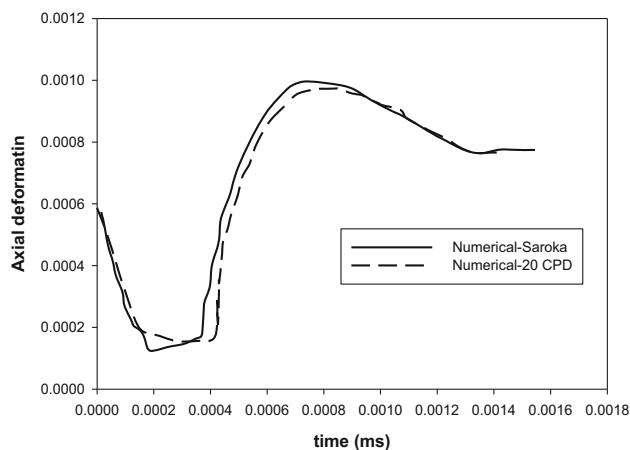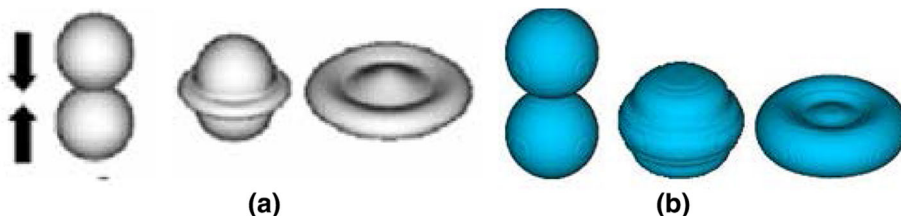
Fig. 4 Compare of axial deformation of numerical simulation and simulation of this study

3.2 Grid independency

In numerical objectives must be done the mesh generation for the geometry of issue at the first steps. The numerical model is based on the finite-difference VOF method. In numerical simulation, the results must be independent from the grid resolution. In other words, the changes in the number of nodes do not have any effect on the results. Non-dimensional elongation is shown in Fig. 5 for different number of grid points. The droplet elongation is almost independent of the numerical solution for the cases of 30 CPD, 32 CPD and 34 CPD (cells per diameter). Therefore, the computational domain with the number of 30 cells per diameters selected to satisfy the accuracy of the code.

3.3 The effects of density ratio

In this section the effect of the density ratio is considered while the droplet diameter is 0.3 mm and the droplet viscosity is 0.001 kg/m.s. The numerical simulation was done for three different density ratios (1, 3 and 6). The cases 1, 2 and 3 in Table 1 were chosen to study the density ratio effect on the collision between two droplets. Figure 6 illustrates the dimensional elongation of the droplets as a function of time after connecting the droplets. The spherical droplets are deformed as they approach each other due to an increase in the fluid gap pressure. The ambient fluid
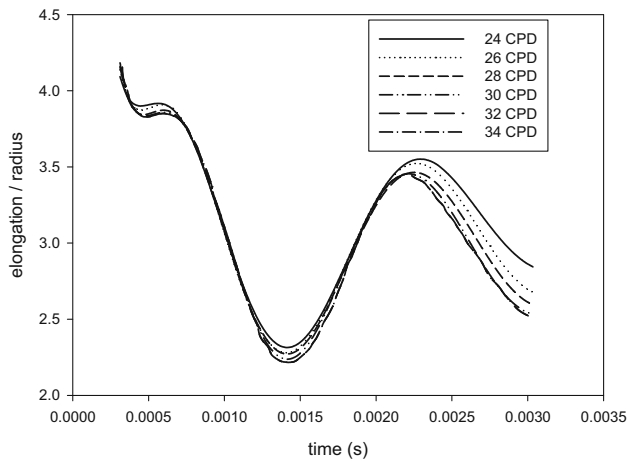
Fig. 3 Deformation of drops (**a**) numerical simulation [18] (**b**) present simulation
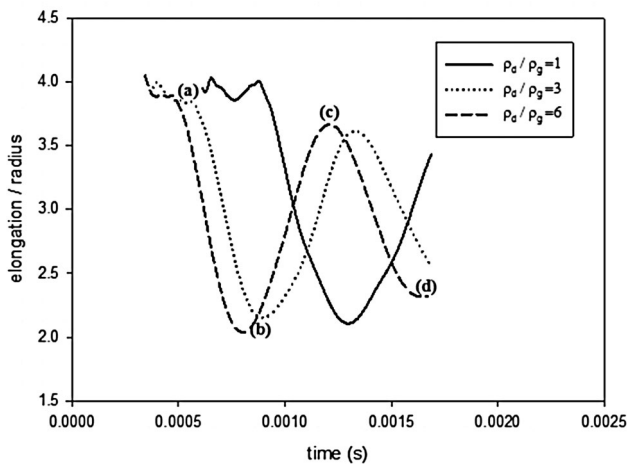
Fig. 5 Independency of the grid

Fig. 6 Non-dimensional elongation of drops for different density ratios, $Re = 107.48$, $We = 0.5$, $\mu_d/\mu_g = 1$, $D_1/D_2 = 1$, $I = 0.16$ (x–z plane)

in the gap between two droplets has a high pressure which it causes the droplet surfaces become flattened. The ambient fluid is entrained into the gap and the droplet kinetic energy is converted to the surface tension energy. The droplet elongation is a sinusoidal curve for all three cases (Fig. 6). The droplets are connected to each other (point *a* in Fig. 6) and converted to a single droplet. Then, the elongation is reduced until the droplet becomes a vertical ellipse. (point *b* in Fig. 6). After that, the elongation is increased because of the conversion of vertical elliptical droplet to horizontal one due to surface tension (point *c* in Fig. 6). The conversion of horizontal ellipse to vertical one is repeated (point *d* in Fig. 6). This process continues periodically until the droplet reaches a spherical shape in stable condition. Higher density ratio causes coalescence to occur faster, so the maximum and minimum elongation values occur in less time. The slope of the graph is the same for all three cases. However, the maximum

elongation amount increases with the density ratio. Additionally, the minimum value of the elongation decreases as the density ratio increases. Figures 7 and 8 show some snapshots of the droplets at different dimensional times for three density ratios. It is observed that the droplet collision time decreases at higher density ratios due to larger inertial force.

3.4 The effect of viscosity ratio

The viscosity ratio effect on the elongation of droplets, deformation and the maximum velocity is investigated in this section (corresponds to the cases 1, 8 and 9 in Table 1). Here, three different viscosity ratios of 1, 20 and 50 are considered. Figure 9 illustrates non-dimensional elongation of droplets after coalescence in x–z plane.

The figure shows that the viscosity ratio has less effect on the elongation than the density ratio. However, the interaction time is the same for different viscosity ratios. As it is described for the case of density ratio, a droplet tends to obtain a spherical shape. This is valid for different viscosity ratios due the effect of surface tension. Therefore, elongation curve has a sinusoidal behavior. It is obvious that the droplet deformation is reduces with increasing the viscosity ratio. Hence, the droplet elongation is the same for high viscosity ratios ($\mu_d/\mu_g = 20$ and 50).

The maximum droplet velocity in x–y–z plane is shown in Fig. 10f after the coalescence occurs. The droplet after merging is two times faster than each single droplet before coalescence. After small fluctuations, the drop reaches its initial velocity of coalescence. This process continues until the droplet becomes a vertical ellipse due to surface tension. During the process the kinetic energy converts to surface energy. The acceleration and deceleration of drop is due to the above energy change. As shown in Fig. 10, the rate of change of maximum velocity is almost the same for three different viscosity ratios. Actually, the maximum velocity of droplet increases slightly with reducing the viscosity ratio.

3.5 The effects of Weber number

To study the effects of Weber number, the cases 4, 6 and 7 in Table 1 are considered. The Weber number (surface tension) varies while the other dimensionless parameters are kept constant. Figure 11 shows the droplet elongation for three different Weber numbers in x–z plane. The amount of kinetic energy is more than surface tension for higher Weber numbers. As shown in Fig. 11, droplet coalescence occurs more slowly at higher Weber number (lower surface tension). The coalescence time is 1.0489, 1.598 and 2.422 ms for the Weber number of 0.53, 1.063 and 2.126, respectively, that reflects that slower process of droplet impact occurs at smaller Weber numbers. As the

Fig. 7 Drop deformation for different density ratios, $Re = 107.48$, $We = 0.5$, $\mu_d/\mu_g = 1$, $D_1/D_2 = 1$, $I = 0.16$ (y–z plane)
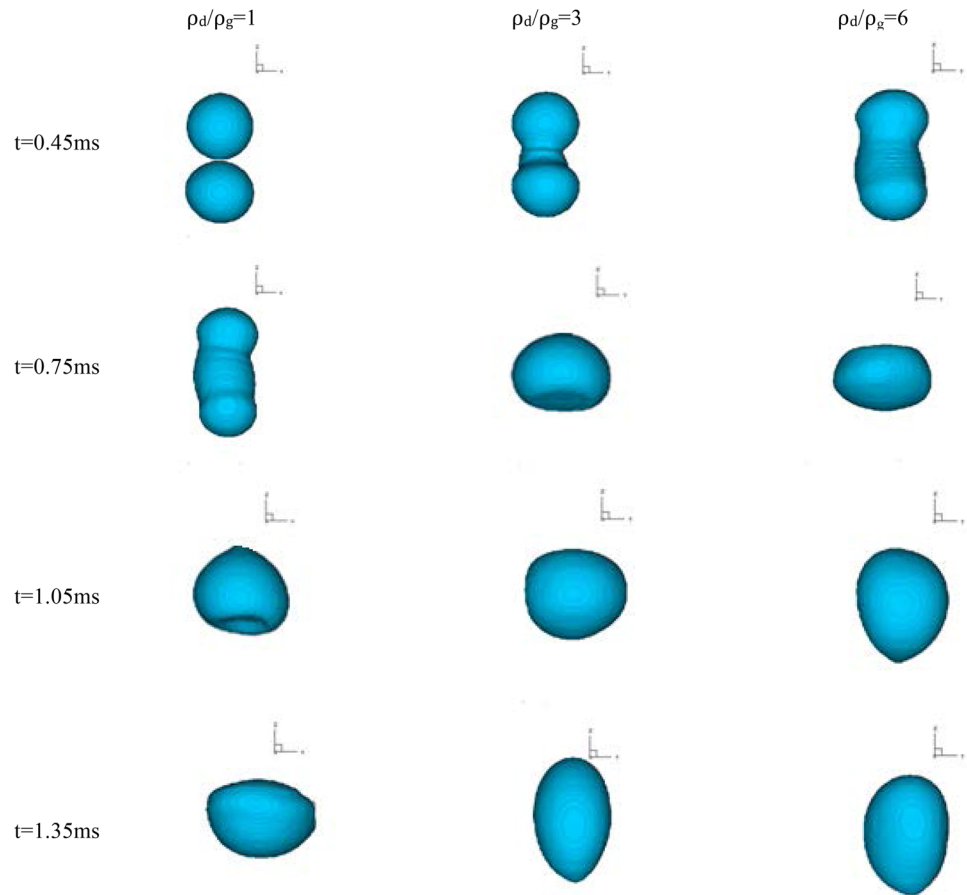
Weber number increases, the minimum and maximum values of the elongation increases. On the other hand, the drop elongation is an increasing function of Weber number.

The maximum velocity of droplets in the plane x–y–z is shown in Fig. 12. It is observed that as the Weber number increases the maximum magnitude of the curves occurs at a longer time. Also Figs. 13 and 14 show the minimum and maximum elongation for different Weber numbers. It is found that the correlation between the droplet elongation and Weber number can be defined as Eqs. 9 and 10.

$$\frac{\text{elongation}_{max}}{\text{radius}} = -0.066(We)^4 + 0.44(We)^3 \\ - 1.116(We)^2 + 1.363(We) + 2.193, \quad (9)$$

$$\frac{\text{elongation}_{min}}{\text{radius}} = 0.113(We)^4 - 0.731(We)^3 + 1.591(We)^2 \\ - 1.233(We) + 2.394. \quad (10)$$

3.6 The effects of Reynolds number

In this section, the effect of Reynolds number is studied. Figure 15 illustrates non-dimensional droplet elongation

for three different Reynolds numbers in the x–z plane (The cases 1, 4 and 5 in Table 1). As shown in this figure the droplets are connected faster at higher Reynolds numbers. The time of droplet impact is 1.021, 1.041 and 1.128 ms for Reynolds number of 107.48, 53,741 and 26.870, respectively. Although the minimum magnitude of the elongation is the same for different Reynolds numbers, but its maximum value increases with increasing the Reynolds number. Figure 16 shows the maximum velocity of droplets after coalescence for three different Reynolds numbers on the x–y–z plane. The maximum droplet velocity is an increasing function Reynolds number. Hence, the droplet needs more kinetic energy at higher Reynolds numbers to change their shapes. Figures 17 and 18 show the snap shots of droplets in x–z and y–z planes, respectively. The figures demonstrate that the droplets coalescence time increases as the Reynolds number increases due to an increase in droplet deformation.

3.7 The effects of impact factor

The effect of impact factor on droplet elongation and droplet deformation is studied (the cases 6, 12 and 13 in Table 1). Figure 19 shows the droplets elongation as a

Fig. 8 Drop deformation for different density ratios, $Re = 107.48$, $We = 0.5$, $\mu_d/\mu_g = 1$, $D_1/D_2 = 1$, $I = 0.16$ (x–z plane)
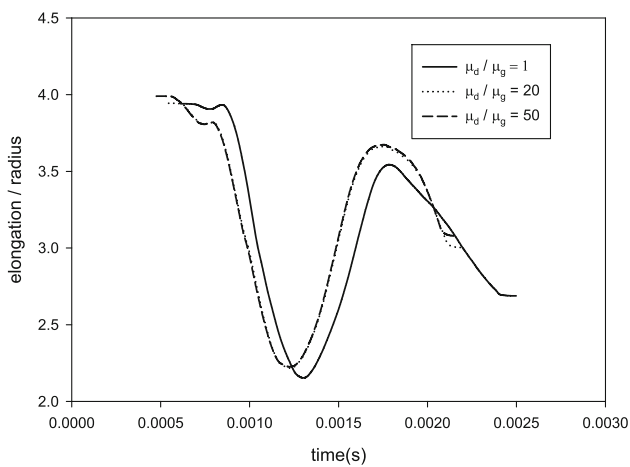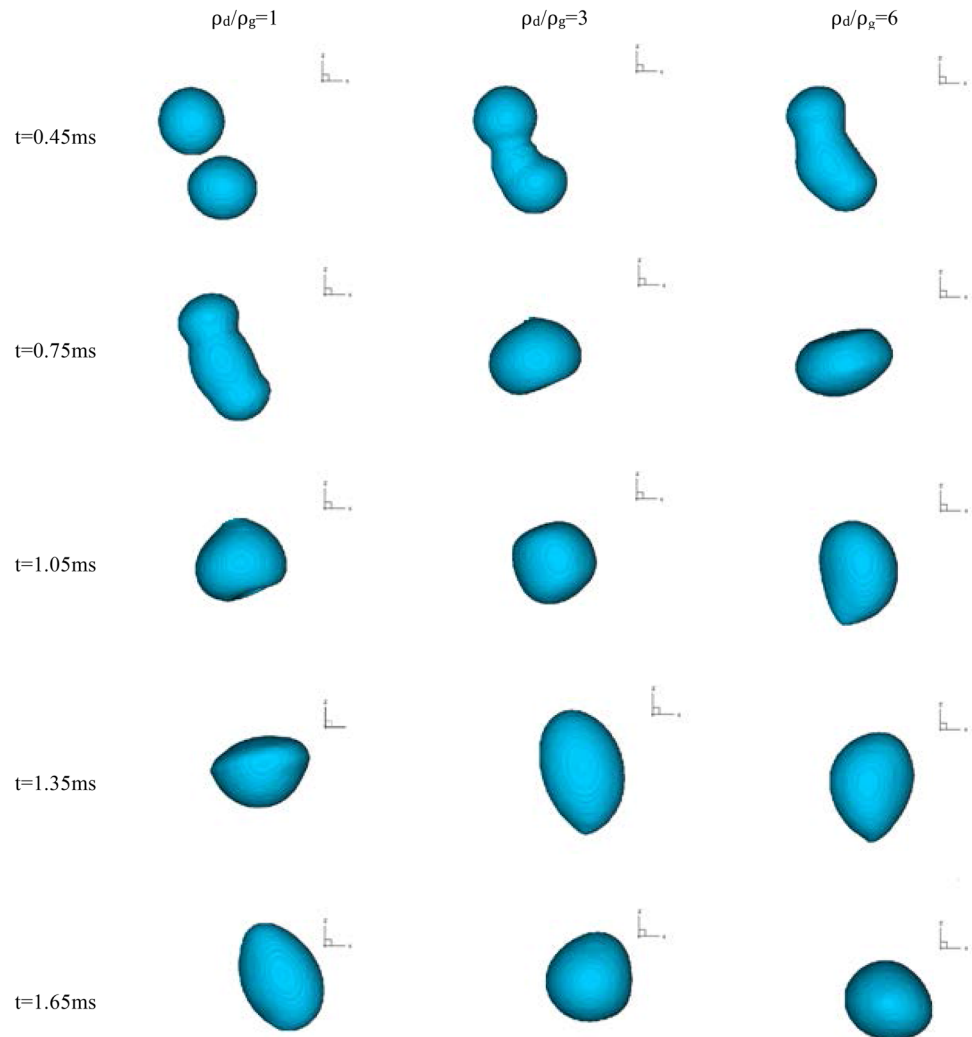

Fig. 9 Non-dimensional elongation of drops for different viscosity ratios, $Re = 107.48$, $We = 0.5$, $\rho_d/\rho_g = 1$, $D_1/D_2 = 1$, $I = 0.16$ (x–z plane)
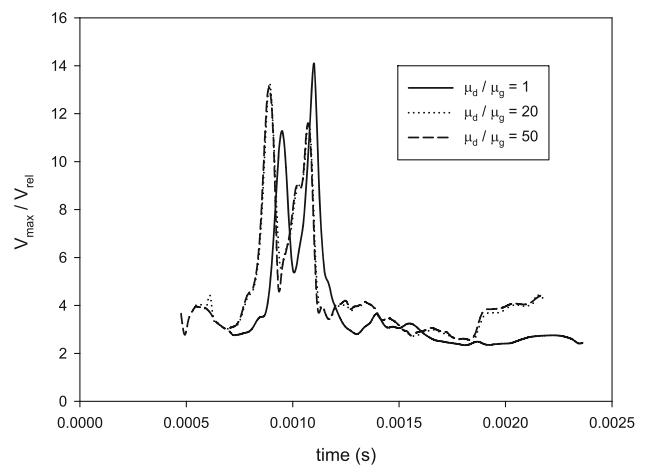

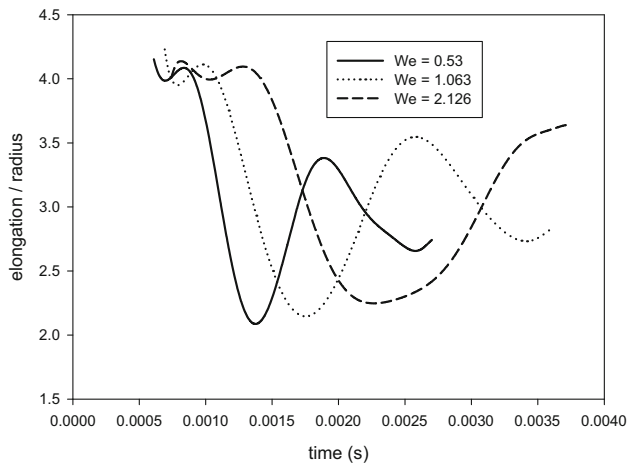**Fig. 10** Non-dimensional maximum relative velocity of drops at different viscosity ratios, $Re = 107.48$, $We = 0.5$, $\rho_d/\rho_g = 1$, $D_1/D_2 = 1$, $I = 0.16$ (x–y–z plane)

Fig. 11 Non-dimensional elongation of drops at different Weber number, $Re = 53.74$, $\mu_d/\mu_g = 1$, $\rho_d/\rho_g = 1$, $D_1/D_2 = 1$, $I = 0.16$ (x–z plane)
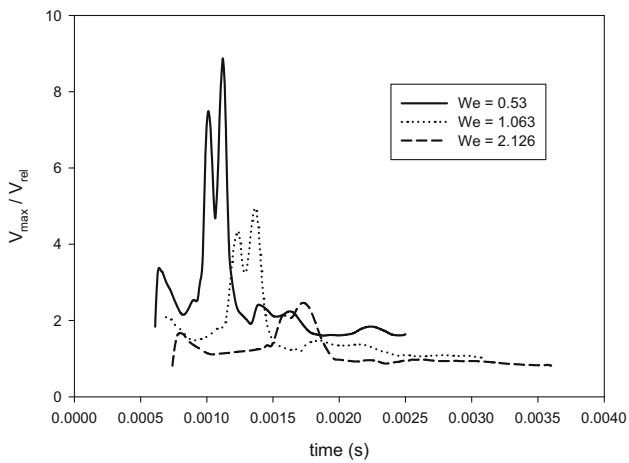

Fig. 12 Non-dimensional maximum relative velocity of drops at different Weber number, $Re = 53.74$, $\mu_d/\mu_g = 1$, $\rho_d/\rho_g = 1$, $D_1/D_2 = 1$, $I = 0.16$ (x–y–z plane)

Fig. 13 Maximum elongation of drops as a function of We number
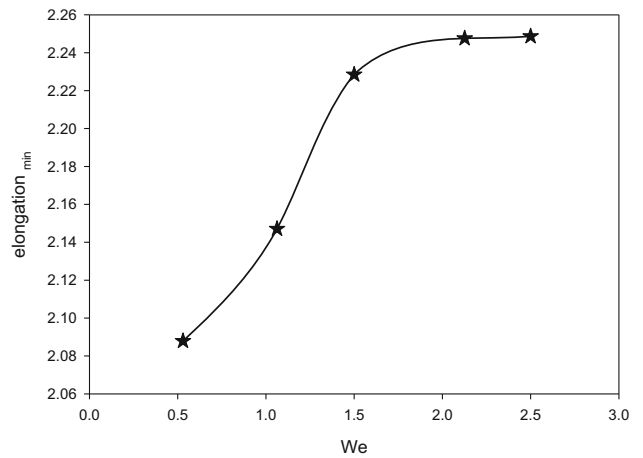
Fig. 14 Minimum elongation of drops as a function of We number
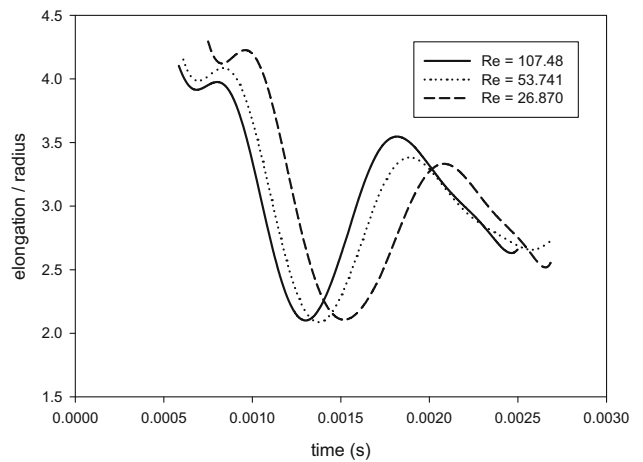

Fig. 15 Non-Dimensional elongation of drops at different Reynolds number, $We = 0.53$, $\mu_d/\mu_g = 1$, $\rho_d/\rho_g = 1$, $D_1/D_2 = 1$, $I = 0.16$ (x–z plane)
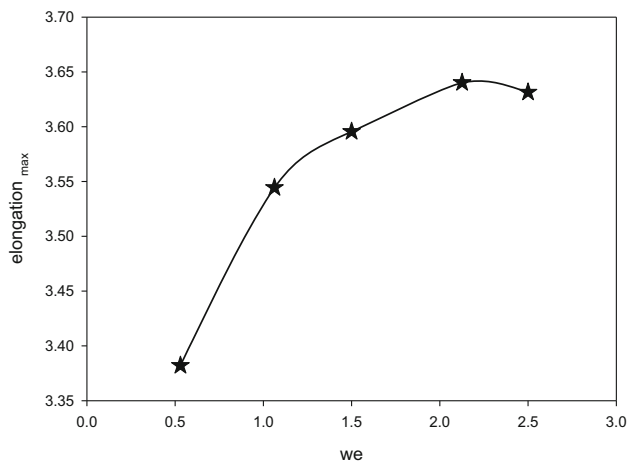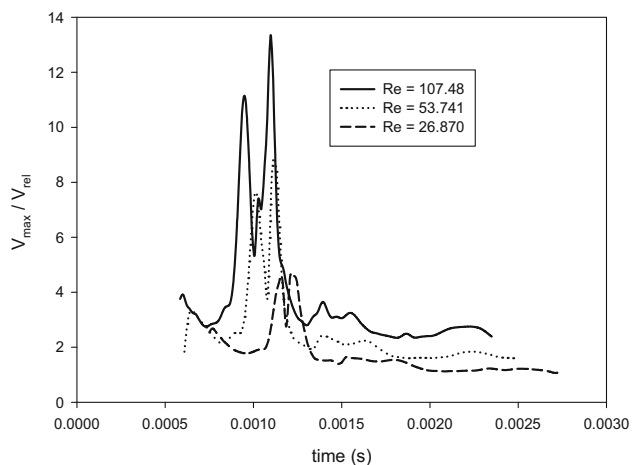

Fig. 16 Non-dimensional maximum relative velocity of drops at different Reynolds number, $We = 0.53$, $\mu_d/\mu_g = 1$, $\rho_d/\rho_g = 1$, $D_1/D_2 = 1$, $I = 0.16$ (x–y–z page)

Fig. 17 Drop deformation at different Reynolds numbers, $We = 0.53$, $\rho_d/\rho_g = 1$, $\mu_d/\mu_g = 1$, $D_1/D_2 = 1$, $I = 0.16$ (x–z plane)
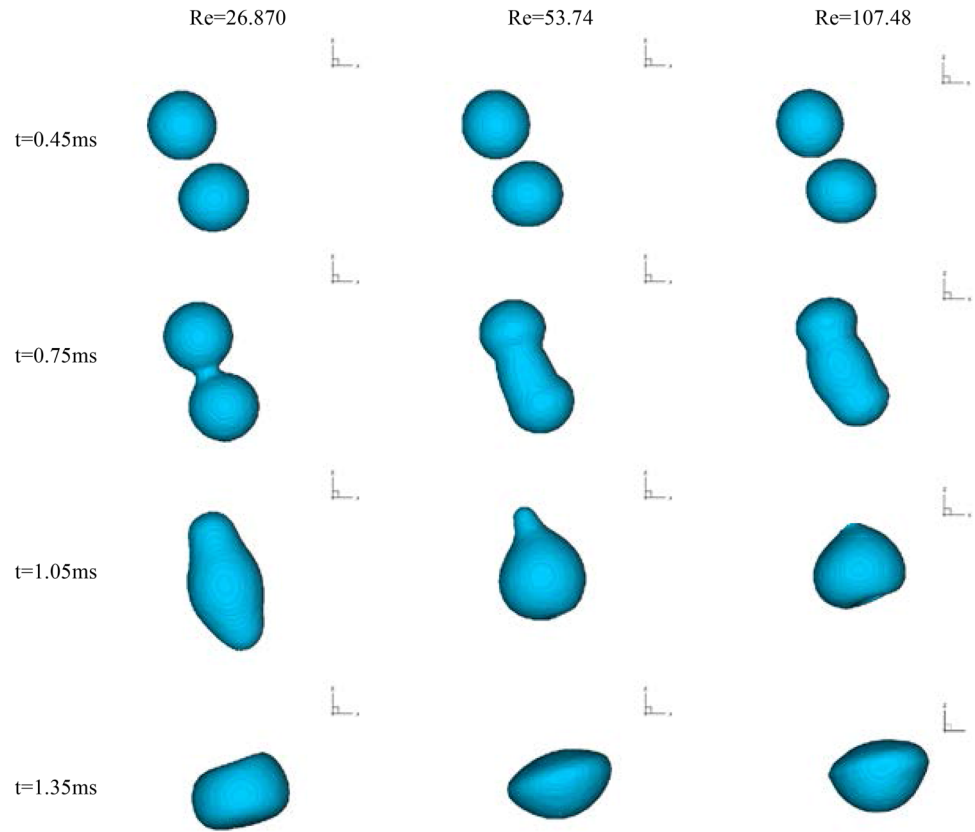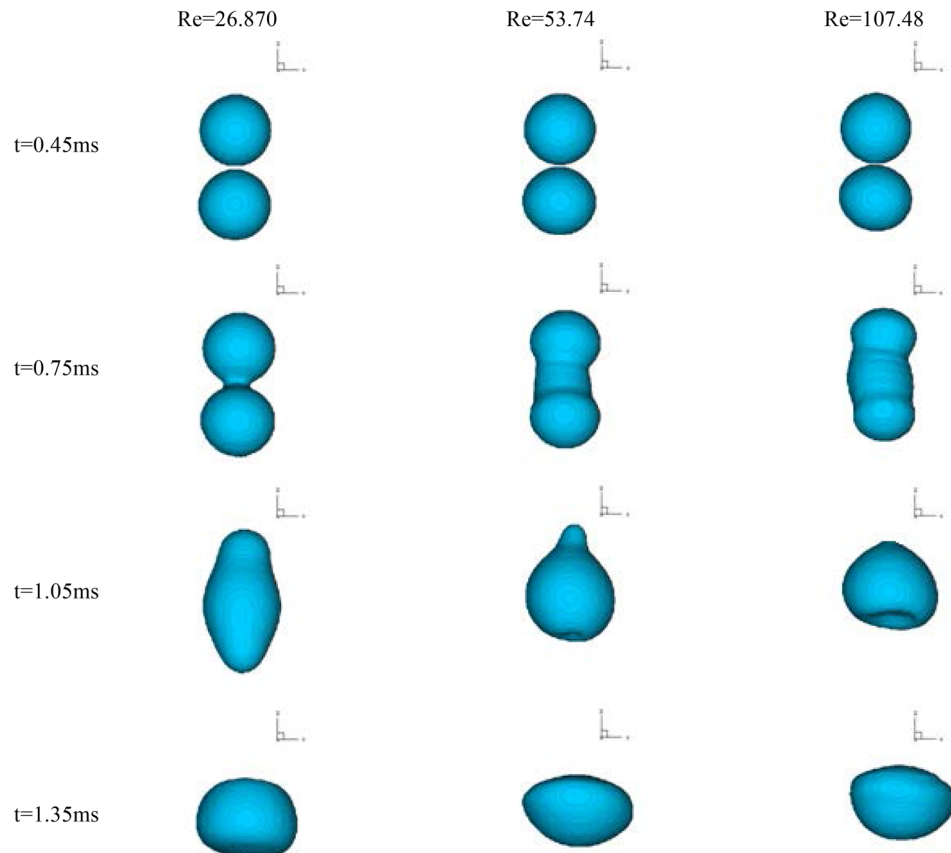

Fig. 18 Drop deformation at different Reynolds numbers, $We = 0.53$, $\rho_d/\rho_g = 1$, $\mu_d/\mu_g = 1$, $D_1/D_2 = 1$, $I = 0.16$ (y–z plane)
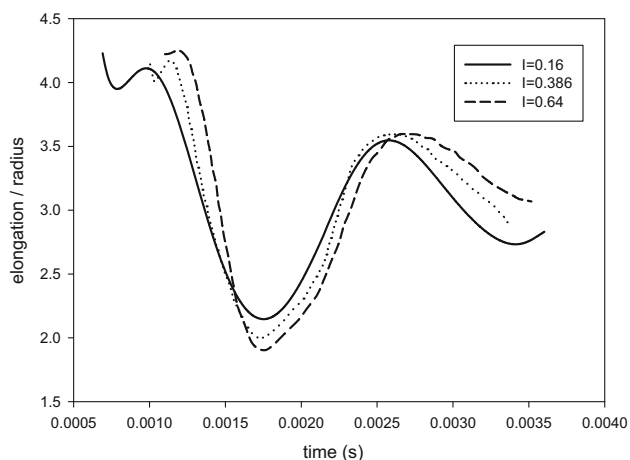
Fig. 19 Non-dimensional elongation of drops at different Impact factors, $We = 1.63$, $Re = 53.741$, $\mu_d/\mu_g = 1$, $\rho_d/\rho_g = 1$, $D_1/D_2 = 1$ (x–z plane)

function of time. It is found that the impact factor has a significant effect on elongation. Although the maximum elongation is almost the same for all cases, but the minimum elongation is smaller for larger impact factors.

4 Conclusions

In the present paper, coalescence phenomena of two off-center water droplets was numerically investigated for fully developed, laminar, unsteady and incompressible flow. A Volume-f Fluid method was used to simulate the motion of droplets. The effect of Weber number, Reynolds number, density ratio, viscosity ratio, and impact factor on the droplet elongation and maximum velocity of them were investigated. In general, the results can be summed up as follows:

1. The droplet elongation is a sinusoidal curve for different density ratios. Higher density ratio causes coalescence to occur faster, so the maximum and minimum elongation values occur in less time.
2. The effect of viscosity ratio is less than that of the density on droplets elongation. Although maximum magnitude of the elongation increases with the viscosity ration, but higher viscosity ratios have less effect on the droplet elongation.
3. It is observed that as the Weber number increases the maximum magnitude of the curves occurs at a longer time. Two correlation functions are found for maximum and minimum values of elongation as a function of Weber number.
4. Although the minimum magnitude of the elongation is the same for different Reynolds numbers, but its maximum value increases with increasing the

Reynolds number. It is found that the impact factor has a significant effect on elongation.

References

1. Ashgriz N, Givi P (1989) Coalescence efficiencies of fuel droplets in binary collisions. Int Commun Heat Mass Transfer 16:11–20
2. Hyun J, Hwang W, Chongyoup (2012) Numerical simulations of the impact and spread in of a particulate droplet on a solid substrate. Model Simul Eng 21:1–10
3. Bayareh M, Mortazavi S (2009) Numerical simulation of the motion of a single drop in a shear flow at finite Reynolds numbers. Iran J Sci Technol Transact B Eng 33:441–452
4. Bayareh M, Mortazavi S (2013) Equilibrium position of a buoyant drop in Couette and Poiseuille flows at finite Reynolds numbers. J Mech 20:53–58
5. Krause F, Li X, Fritsching U (2011) Simulation of droplet-formation and interaction in emulsification processes. Eng Appl Comput Fluid Mech 5:406–415
6. Qian J, Law CK (1997) Regimes of coalescence and separation in droplet collision. J Fluid Mech 331:59–80
7. Wierzba A (1990) Deformation and breakup of liquid droplets in a gas stream at nearly critical Weber numbers. Exp Fluids 9:59–64
8. Ashgriz N, Poo JP (1990) Coalescence and separation in binary collisions of liquid droplets. J Fluid Mech 221:183–204
9. Seevaratnam GK, Ding H, Michel O, Heng JYY, Matar OK (2010) Laminar flow deformation of a droplet adhering to a wall in a channel. Chem Eng Sci 65:4523–4924
10. Renardy Y (2007) The effects of confinement and inertia on the production of droplets. Rheol Acta 46:521–529
11. Kékesi T, Amberg G, Wittberg L (2014) Droplet deformation and breakup. Int J Multiph Flow 66:1–10
12. Ioannou N, Liu H, Zhang YH (2016) Droplet dynamics in confinement. J Comput Sci 17:463–474
13. Feigl K, Tanner F, Holzapfel S, Windhab E (2014) Effect of flow type, channel height, and viscosity on droplet production from micro-pores. Chem Eng Sci 116:372–382
14. Bayareh M, Mortazavi S (2011) Effect of density ratio on the hydrodynamic interaction between two drops in simple shear flow. Iran J Sci Technol Transact B Eng 35:121–132
15. Bayareh M, Mortazavi S (2011) Binary collision of drops in simple shear flow at finite Reynolds numbers: geometry and viscosity ratio effects. Adv Eng Softw 42:604–611
16. Nobari MRH, Tryggvason G (1996) Numerical simulation of three-dimensional droplet collisions. Am Instit Aeronaut Astronaut 34(4):750–755
17. Melean Y, Sigalotti LDG (2005) Coalescence of colliding van der Waals liquid droplets. Int J Heat Mass Transf 48:4041–4061
18. Nikolopoulos N, Theodorakakos A, Bergeles G (2009) Off-centre binary collision of droplets: a numerical investigation. Int J Heat Mass Transf 52:4160–4174
19. Saroka MD, Ashgriz N, Movassat M (2012) Numerical investigation of head-on binary droplet collisions in a dynamically inert environment. J Appl Fluid Mech 5:23–37
20. Krishnan KG, Loth E (2015) Effects of gas and droplet characteristics on droplet-droplet collision outcome regimes. Int J Multiph Flow 77:171–186
21. Ahmadi Nadooshan A, Shirani E (2008) Interface pressure model for surface tension force for VOF-based methods in interfacial flows. Eng Appl Comput Fluid Mech 2(4):496–513